Spontaneous birefringence in boracites. Measurements and applications

Schmid, Hans; Tippmann, Heinz

How to cite

SCHMID, Hans, TIPPMANN, Heinz. Spontaneous birefringence in boracites. Measurements and applications. In: Ferroelectrics, 1978, vol. 20, n° 1-2, p. 21–36. doi: 10.1080/00150197808239427

This publication URL: https://archive-ouverte.unige.ch/unige:33390
Publication DOI: 10.1080/00150197808239427

Ferroelectrics
1978, Vol. 20, pp. 21–36

SPONTANEOUS BIREFRINGENCE IN BORACITES–MEASUREMENTS AND APPLICATIONS

H. SCHMID† and H. TIPPMANN

Battelle Geneva Research Laboratories, CH-1227 Carouge-Geneva, Switzerland

(Received September 18, 1977)

The techniques and results of measurements of the spontaneous birefringence versus temperature are discussed for the fully ferroelectric/fully ferroelastic phases of Mg–Cl, Cr–Cl, Mn–Cl, Mn–Br, Mn–I, Fe–Cl, Fe–Br, Fe–I, Co–Cl, Co–Br, Co–I, Ni–Cl, Ni–Br, Cu–Cl, Cu–Br, Zn–Cl, Zn–Br, Zn–I, Cd–Cl, Cd–Br and Cd–I boracites. Three types of phase sequence occur: $\bar{4}3m \leftrightarrow mm2 \leftrightarrow m \leftrightarrow 3m$ (Fe–Cl, Fe–I, Co–Cl, Zn–Cl), $\bar{4}3m \leftrightarrow mm2 \leftrightarrow 3m$ (Fe–Br) and $\bar{4}3m \leftrightarrow mm2$ (all other compositions). All transitions are of first order. The magnetic ones are excluded from discussion.

Crystallophysical and potential technological applications of the spontaneous birefringence are commented:

— Light gates (display, page composers, holographic storage): the favorable symmetry species $43mFmmm2$, $43mFm$, $43mF3m$ and the high spontaneous birefringence of boracites allow light gate devices with longitudinal electrode configuration. Feasibility studies on single crystalline Fe–I and of epitaxial growth of Ni–Cl boracite show that the development of zero shear compositions is mandatory. Potential ways of their realization are discussed.

— The study of the statics and dynamics of domains and of their walls.

— The obligatory simultaneous optical control of the sample state during physical measurements, which is considered for the time being as one of the most important applications of spontaneous birefringence of boracites.

1 INTRODUCTION

Boracites form a large crystal family[1–3] with the general formula $M_3B_7O_{13}X$, where M stands for Mg, Cr, Mn, Fe, Co, Ni, Cu, Zn, Cd and X for OH, F, Cl, Br, I, NO_3,[4] S, Se and Te. If M equals lithium, the formula becomes $Li_4B_7O_{12}X$ for X being a halide,[5] and $Li_5B_7O_{12}X$ for X being a chalcogenide.[6]‡

Most—but not all—compositions transform from a cubic high temperature phase (point group $\bar{4}3m$) to one or to a sequence of "fully ferroelectric"/"fully ferroelastic" (for nomenclature, see Ref. 7) phases with point symmetry $mm2$, m and $3m$.[8,9] At low temperatures many of them become ferromagnetoelectric (see Ref. 9, p. 135).

At the temperatures of the onset of the ferroelectric/ferroelastic phases the spherical optical indicatrix of the cubic phase deforms "spontaneously", and in accord with the symmetry of these phases becomes a rotational ellipsoid ($3m$) or a triaxial ellipsoid ($mm2$, m). We are interested in the magnitude, orientation and temperature dependence, and in the technological and scientific applications of the spontaneous birefringence, Δn_s, in the principal sections of the indicatrix ellipsoids, and we call it "spontaneous" in analogy to spontaneous polarization, spontaneous deformation, etc.

2 HISTORICAL REMARKS[10–12]

Volger remarks in his monograph on boracite (1855) that the children of the German town Lüneburg probably are the discoverers of boracite. They certainly played at dice with their "Würfelstein" long before G. S. O. Lasius officially discovered "Cubic Quartz" on Lüneburg's nearby "Kalkberg" (1787). Since Westrumb (1788) found that the material contains boric acid, Mg and Ca, Werner baptized the mineral "Boracite" (1789).

The mineral boracite, $Mg_3B_7O_{13}Cl$, is orthorhombic, hence birefringent below 265°C. Some well-grown specimens show beautiful large domains, but the majority complicated lamellar configurations. This was a tantalizing problem for researchers in the past century.

† New address: University of Geneva, Department of Inorganic, Analytical and Applied Chemistry, Sciences II, CH-1211 Geneva 4, Switzerland.

‡ In this paper the boracite compositions will be abbreviated by M–X.

As early as 1821 Sir David Brewster found that "from the optical point of view boracite does not satisfy the requirements of the regular system", he thought boracite to be optically uniaxial and trigonal. Then B. Biot (1841) tried to explain the anomalous birefringence of cubic crystals by their composition as a set of plates, acting similarly on polarized light as a set of glass-plates. Once the famous crystallographer Franz E. Neumann had discovered (1841) that optically isotropic bodies may become birefringent owing to uniaxial pressure or to a thermal gradient, Marbach (1855) took up this idea and thought the birefringent layers of boracite were due to a pressure acting during crystallization. Others followed step (Reusch, Klocke 1880). Volger (1854) tried to prove that lamellar birefringent inclusions—"Parasite"—are formed during some kind of pseudomorphosis. This idea was tenacious: Decloiseaux still advocated it in 1863 and Klein in Göttingen (1880, 1881) claimed obstinately that a skeleton of parasite forms first and that boracite comes next. In the meantime Greinitz (1876) realized that even fresh and undecomposed boracite birefringent. Mallard in Paris (1876) carefully measured extinction directions and the principal refractive indices, and he was finally able to give the correct answer: boracite is a twinned aggregate of differently oriented blocks or lamellas of orthorhombic parts. He also was the first to state qualitatively (1882) that "the strength of the birefringence decreases with increasing temperature" and disappears at 265°C. After a vehement exchange of opinions between Klein and Mallard, Mallard's explanations survived.

3 EXPERIMENTAL

3.1 Sample Preparation

3.1.1 Single crystals and chemistry Except for Mg–Cl boracite, a natural crystal of which—from Eime–Hannover†—was used, all single crystals were grown by gas phase transport.[13] The natural crystals contained tiny amounts of Mn^{++}, as detected by EPR.[14]

3.1.2 Crystal platelets Two principal sections of the *mm*2 indicatrix lie in cubic (110) planes and the third one in a cubic (100) plane, one of the principal sections of the *m* phase (⊥ b-axis) and the sole principal section of the 3*m* phase lie in cubic (110) planes, therefore only platelets cut parallel to cubic (100) and (110) and polished with 1 μm diamond paste were prepared with 30 to 100 μm thickness for the higher birefringence compositions (e.g. Cl and Br boracites) and with up to 400 μm for small birefringence compositions (e.g. Fe–I, Mn–I, Zn–I).

3.1.3 Preparation of single domains The requirement of stress freeness of the samples for the correct measurement of spontaneous birefringence, Δn_s, of ferroelectric/ferroelastic phases necessitates fully poled samples or stress free domain patterns. One or another of the following methods was used to fulfil this requirement.

3.1.3.1 Electric field poling In the present study electric field poling was applicable in the case of the *mm*2 phases only. The polished and etched platelets were electroded after outgassing (~400°C) in ultra high vacuum by means of a transparent gold layer, deposited after applying a short flash of chromium in order to increase adherence. Two sample forms were used:

— $(100)_{cub}$ cut thin platelets for measuring Δn_s perpendicular to P_s

— $(110)_{cub}$ cut rectangular platelets with the short dimension parallel $[100]_{cub}$ for measuring Δn_s in the orthorhombic *a*, *c* and *b*,*c* planes, as described earlier.[15] Depending upon the resistivity of the material, both cooling in an electric field through T_c and switching more or less below T_c were used for poling.

3.1.3.2 Ferroelastic poling of the mm2 phase In the *mm*2 phase of boracites (Aizu species 43*mFmm*2) single domains can be obtained by applying stress along $[110]_{cub}$. For this purpose some thick (400 μm) $(100)_{cub}$ cut samples (Table I) were squeezed by means of micro jaws. Simultaneous observation along $[001]_{cub}$ under the polarizing microscope is mandatory to avoid cracking. The method is useful if high electric conductivity, e.g. above 200°C, impedes electric poling. Saturation is usually achieved in the central part of the samples only, owing to inhomogeneous stress.

3.1.3.3 Domain size enhancement by annealing and temperature cycling If poling by stress or electric field is not applicable, annealing above the

† Courtesy of Professor Saalfeld, Institute for Mineralogy, Hamburg University.

TABLE I

Methods used for obtaining single domains for measuring spontaneous birefringence

Boracite	Phase	Electric field poling: E [10^5 Vm^{-1}]	Electric field poling: thickness [μm]	Electric field poling: temp. [°C]	Stress // [110]$_{cub}$ temperature [°C]	Temperature cycling through T_c	as-grown state
Mg-Cl	*mm*2				100	x	x
Cr-Cl	*mm*2	90	50	- 59			
Mn-Cl	*mm*2	143		25			x
Mn-Br	*mm*2	111	72	25			
Mn-I	*mm*2	14	364	100-120			
Fe-Cl	*mm*2				300	x	x
	m					x	
	$\bar{4}3m$					x	
Fe-Br	*mm*2				160	x	x
	$\bar{4}3m$					x	
Fe-I	*mm*2		100,300	25	25	x	x
Co-Cl	*mm*2					x	x
	m					x	
	$\bar{4}3m$					x	
Co-Br	*mm*2	130	30	150			
Co-I	*mm*2	67	48,60	-85			
Ni-Cl	*mm*2	20	100	25			x
Ni-Br	*mm*2				100		x
Cu-Cl	*mm*2	50	80	25	25		
Cu-Br	*mm*2	43	70	-50			
Zn-Cl	*mm*2				360		x
	m					x	
	$\bar{4}3m$					x	
Zn-Br	*mm*2					x	x
Zn-I	*mm*2	30	600	25			
Cd-Cl	*mm*2						x
Cd-Br	*mm*2						x
Cd-I	*mm*2						x

*mm*2/$\bar{4}3m$ phase transition and(or) repeated slow cooling through T_c often yields a convenient size of orthorhombic single domains. The method proves the more successful, the fewer growth centres and polishing defects there are.

The lamellar structure (see Section 4.3) of the trigonal and monoclinic phase cannot be fully reduced by this method; it can be largely simplified, however, if an orthorhombic single domain is produced first.

3.1.3.4 As-grown and as-cooled samples sometimes display large domains (e.g. Ni–Cl, Ni–Br) which can be used directly for measurements (see Table I).

3.2 Measurement Technique

If not otherwise mentioned, Δn_s has been measured at $\lambda = 546$ nm by means of an Ehringhaus compensator[16] and compensating the path difference visually. For measurements vs. temperature the sample was lodged in a silvered quartz Dewar tube with plane parallel windows. The sample bathed in a temperature stabilized (±0.2 deg) nitrogen gas flow. The high T_c compositions were measured on a Leitz-hotstage. The accuracy of the absolute values of Δn_s is usually 1 to 5%.

4 RESULTS

4.1 General Remarks

In Figures 1 to 17 the results of the birefringence vs. temperature measurements are presented. As a rule, endeavours were made to measure Δn_s in all three indicatrix principal sections of the *mm*2 phase, but it has been possible so far to collect Δn_s perpendicular to P_s only for all compositions studied. This is also the most interesting Δn_s for technical applications (see Section 5.4). For some compositions Δn_s of only two principal sections was measurable. Then the third one has been obtained by combining the values of the two measured ones (curves without dots in figures).

It has not been possible to detwin the *m*-phase entirely. Only lamellar packages composed of two kinds of *m*-domain, which originated from one orientation of *mm*2 domain, have been isolated

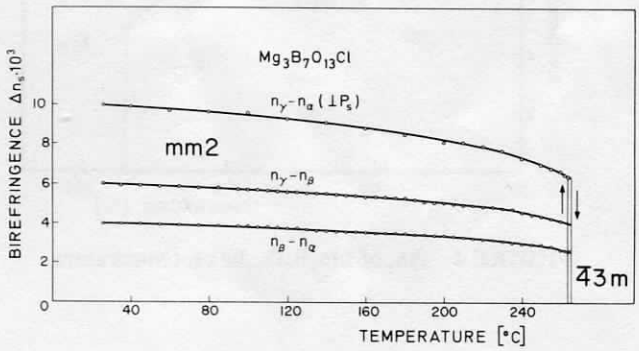

FIGURE 1 Δn_s of $Mg_3B_7O_{13}Cl$ *vs.* temperature (natural crystal from Eime/Hannover).

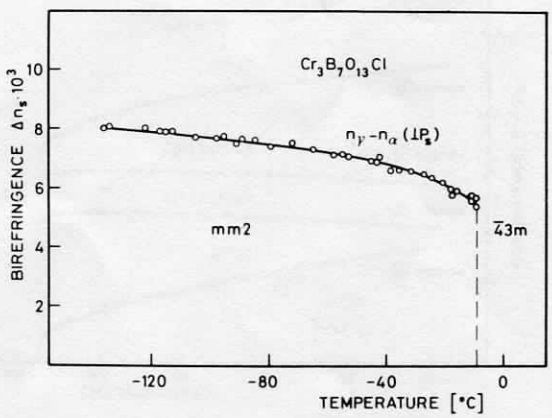

FIGURE 2 Δn_s ($\perp P_s$) of $Cr_3B_7O_{13}Cl$ *vs.* temperature.

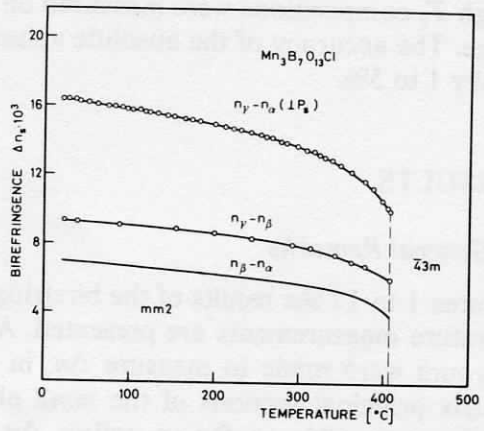

FIGURE 3 Δn_s of $Mn_3B_7O_{13}Cl$ *vs.* temperature.

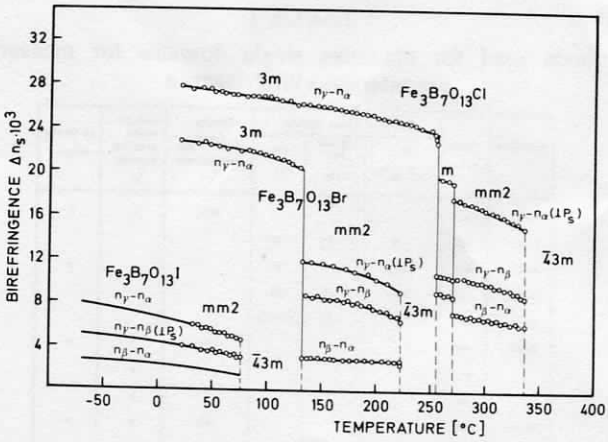

FIGURE 6 Δn_s of $Fe_3B_7O_{13}Cl$, $Fe_3B_7O_{13}Br$ and $Fe_3B_7O_{13}I$ *vs.* temperature.

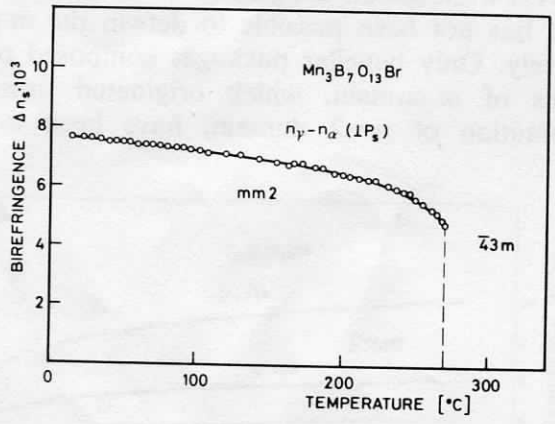

FIGURE 4 Δn_s of $Mn_3B_7O_{13}Br$ *vs.* temperature.

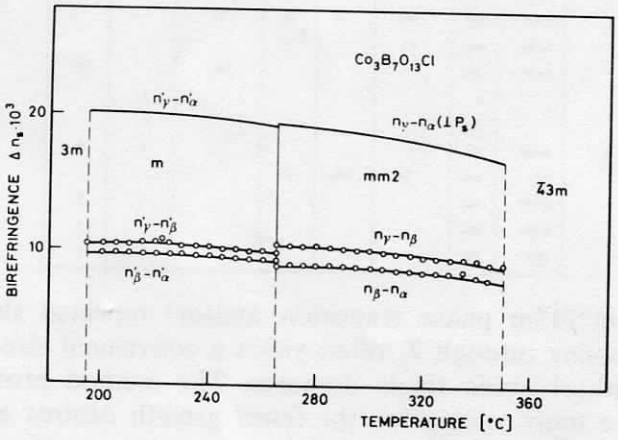

FIGURE 7 Δn_s of $Co_3B_7O_{13}Cl$ *vs.* temperature (data on $3m$ phase are lacking).

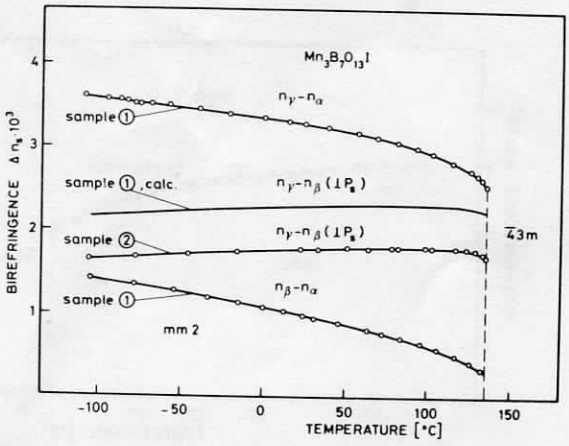

FIGURE 5 Δn_s of $Mn_3B_7O_{13}I$ *vs.* temperature.

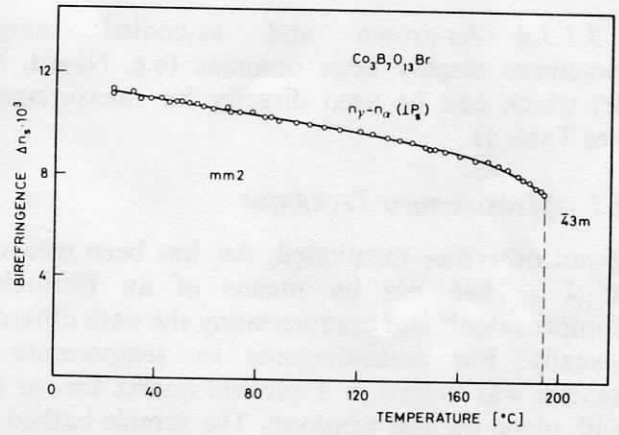

FIGURE 8 Δn_s ($\perp P_s$) of $Co_3B_7O_{13}Br$ *vs.* temperature.

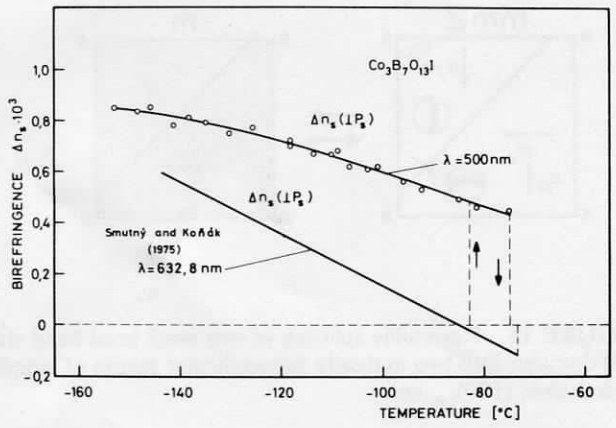

FIGURE 9 Δn_s ($\perp P_s$) of $Co_3B_7O_{13}I$ *vs.* temperature.

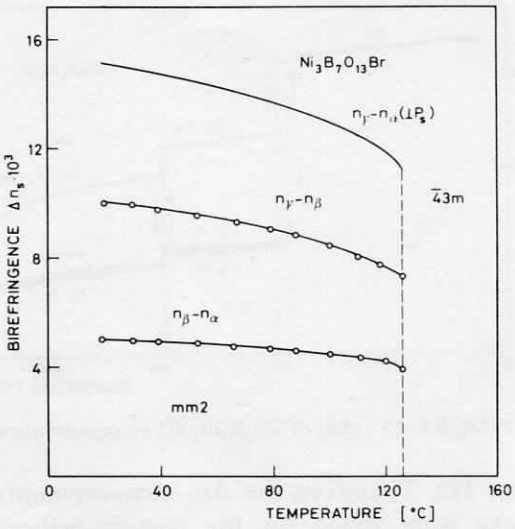

FIGURE 12 Δn_s of $Ni_3B_7O_{13}Br$ *vs.* temperature.

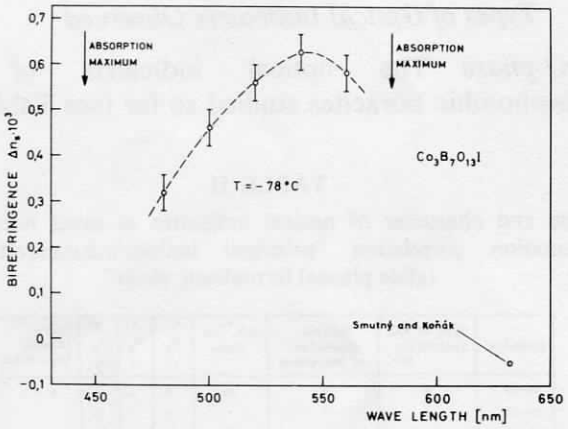

FIGURE 10 Dispersion of Δn_s ($\perp P_s$) of $Co_3B_7O_{13}I$ at −78°C.

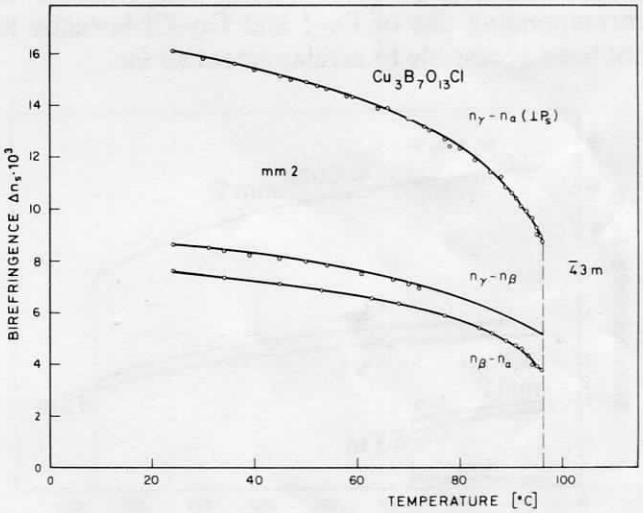

FIGURE 13 Δn_s of $Cu_3B_7O_{13}Cl$ *vs.* temperature.

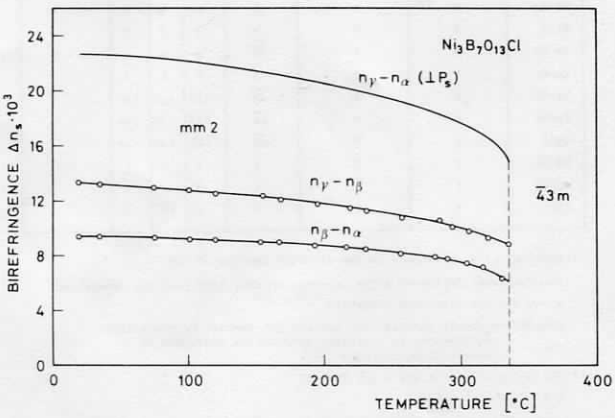

FIGURE 11 Δn_s of $Ni_3B_7O_{13}Cl$ *vs.* temperature.

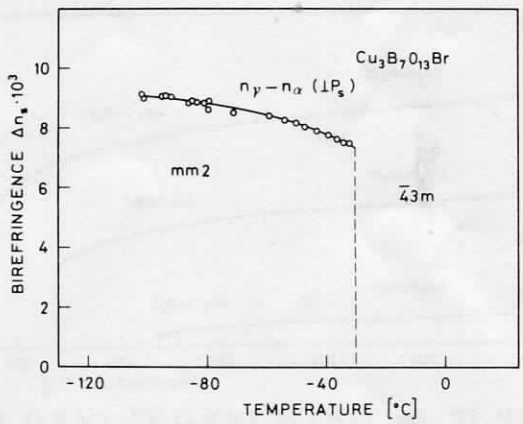

FIGURE 14 Δn_s ($\perp P_s$) of $Cu_3B_7O_{13}Br$ *vs.* temperature.

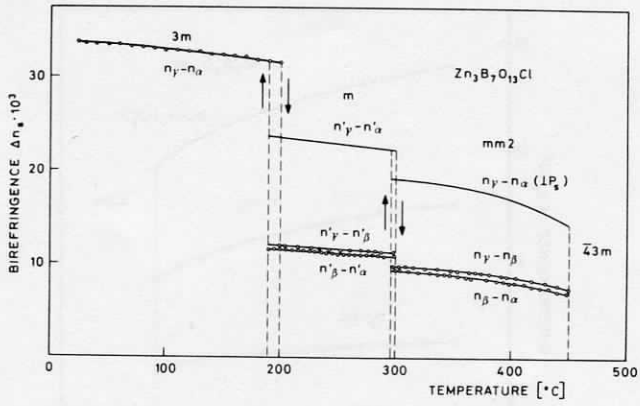

FIGURE 15 Δn_s of $Zn_3B_7O_{13}Cl$ *vs.* temperature.

(Figure 18). Therefore the Δn_s measurements of the *m*-phase were made on the pseudo-orthorhombic principal sections of these stacks of domain.

Spontaneous birefringence of the principal section of trigonal Fe–Cl, Fe–Br and Zn–Cl boracite has been measured (Figure 6 and 15), whereas the corresponding one of Fe–I and Co–Cl boracite has not been accessible to measurement so far.

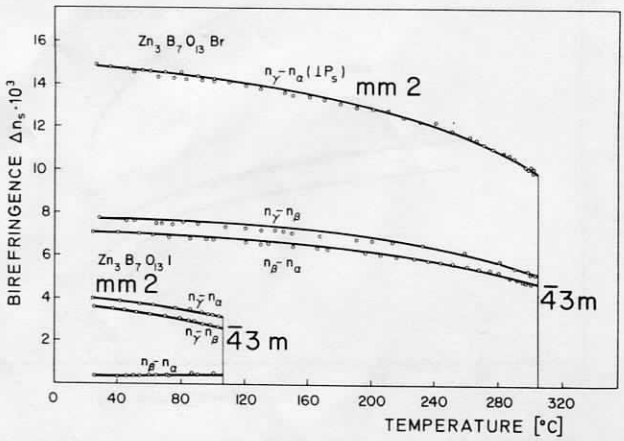

FIGURE 16 Δn_s of $Zn_3B_7O_{13}Br$ and $Zn_3B_7O_{13}I$ *vs.* temperature.

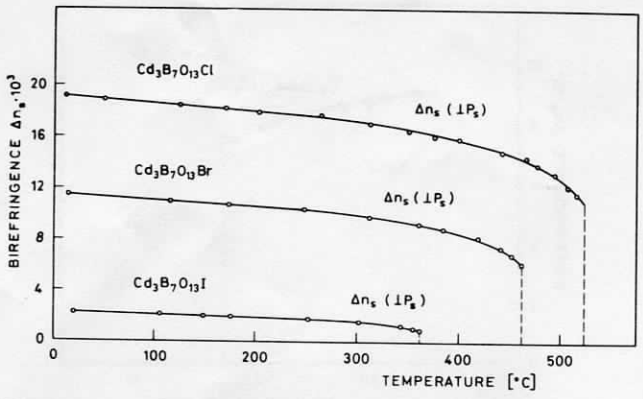

FIGURE 17 Δn_s ($\perp P_s$) of $Cd_3B_7O_{13}Cl$, $Cd_3B_7O_{13}Br$ and $Cd_3B_7O_{13}I$ *vs.* temperature.

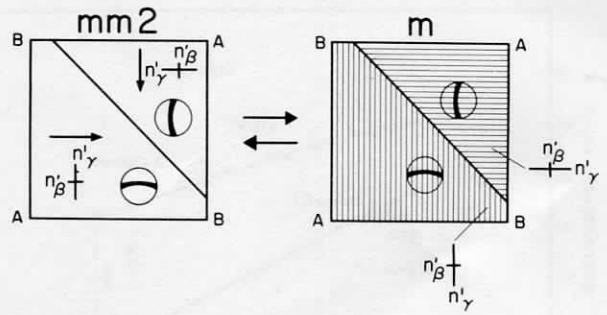

FIGURE 18 Reversible splitting of two *mm*2 head-head (tail-tail) domains into two mutually perpendicular stacks of lamellar *m*-domains; $(100)_{cub}$-cut.

As a rule, Δn_s increases for a series of compositions if the metal ion is kept constant and the halogen is changed in the direction I → Br → Cl. The Curie temperatures increase in the same direction (Figures 6, 16 and 17).

4.2 *Types of Optical Indicatrix Observed*

mm2-phase The optical indicatrix of all orthorhombic boracites studied so far (see Table II)

TABLE II

Type and character of optical indicatrix of *mm*2 boracites; orientation correlation "principal indices/*a*,*b*,*c*-parameters/(glide planes) ferroelastic shear"

Boracite	Type of mm2 indicatrix **)	Optical character of mm2-phase	O.A.*) in plane	*) n_γ //	*) n_α //	*) n_β //	Ferro-*) elastic test gives:
Mg-Cl	A	+	$\bar{a}b$	b	a	c	a > b
Cr-Cl	?	?		?	?	?	
Mn-Cl	A	+	$\bar{a}b$	b	a	c	
Mn-Br	A	+	$\bar{a}b$	b	a	c	
Mn-I	B	+	$\bar{b}c$	b	c	a	
Fe-Cl	A	+	$\bar{a}b$	(b)	(a)	(c)	
Fe-Br	A	+	$\bar{a}b$	(b)	(a)	c	
Fe-I	B	+	$\bar{b}c$	b	c	a	a > b
Co-Cl	A	+	$\bar{a}b$	(b)	(a)	(c)	
Co-Br	A	+	ab	(b)	(a)	(c)	
Co-I	?	?	?	?	?	?	
Ni-Cl	A	+	ab	b	a	c	a > b
Ni-Br	A	+	ab	b	a	c	a > b
Ni-I	?	?	?	?	?	?	
Cu-Cl	A	+	$\bar{a}b$	b	a	c	a > b
Cu-Br	?	?	?	?	?	?	
Zn-Cl	A	+	$\bar{a}b$	(b)	(a)	(c)	
Zn-Br	A	+	$\bar{a}b$	(b)	(a)	(c)	
Zn-I	A	+	$\bar{a}b$	(b)	(a)	(c)	
Cd-Cl	?	?	?	?	?	?	
Cd-Br	?	?	?	?	?	?	
Cd-I	?	?	?	?	?	?	

* Here, a, b, c correspond to the standard setting of the International Tables of x-Ray Crystallography. Note that the convention a < b < c has been used elsewhere [54],[32]

Brackets: probable correlation, but not yet checked by precession photographs; no brackets: correlation confirmed by precession photographs [21]

** For definition of A and B see Fig. 19

O.A. = optical axes

Nota: Information on the mutual orientation of indicatrix, ferroelastic shear, sense of P_s and etch figures is found in ref. [32].

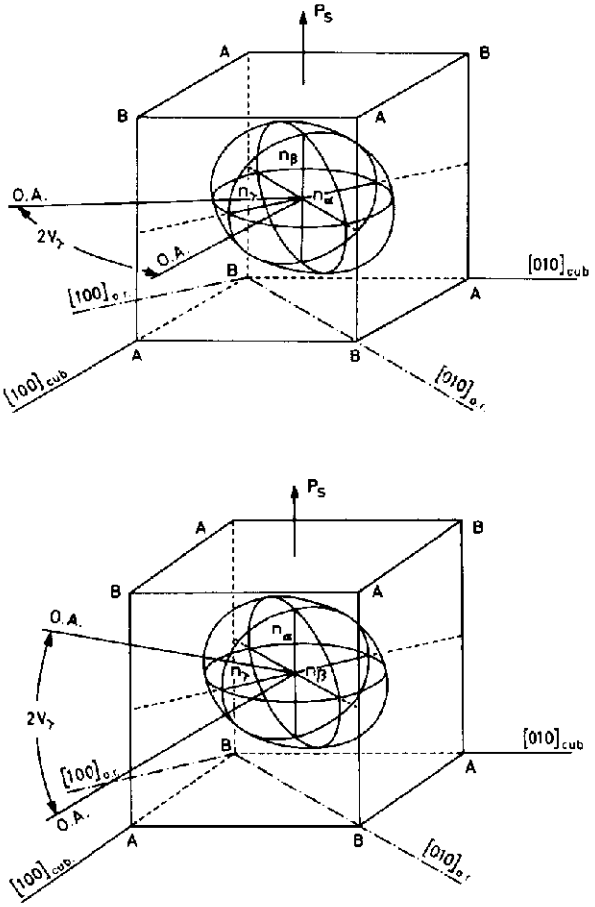

FIGURE 19 Type "A" and "B" of optical indicatrix of *mm*2 boracites (compare Table II) (a) type A, (b) type B.

is *biaxial positive*. However, two types thereof can be found:

Type A: the optical axes lie in the *a*, *b*-plane, i.e. perpendicular to P_s (Figure 19a), with n_β parallel to P_s and n_α and n_γ parallel to the orthorhombic *a* and *b* axes, respectively, if *a*, *b* and *c* are defined by the standard setting of the International Tables of Crystallography. All chlorine and bromine boracites seem to belong to this type.

Type B: the optical axes lie in the *b*, *c*-plane with n_γ parallel *b* and n_α parallel P_s (*c*-axis) (Figure 19b). This type is known so far for Fe–I and Mn–I boracite, and is supposed to occur in other iodine-boracites.

m-phase The type of indicatrix of the *m*-phase has not been elucidated so far because detwinning has not been achieved. There is, however, orthoscopic and conoscopic evidence that its form and orientation are very close to that of the *mm*2 phase (Figure 18).

3m-phase The optical character of the uniaxial index ellipsoid of the 3*m*-phase of Fe–Cl, Fe–Br and Zn–Cl boracite, is negative.[17] That of the 3*m*-phase of Co–Cl and Fe–I boracite is probably negative, too.

4.3 Relation Between the Domain Orientation in the Phase Sequence mm2 ⇄ m ⇄ 3m

The difference in magnitude of Δn_s of the *mm*2-phase and the pseudo-orthorhombic one of the *m*-phase of a certain composition is usually very small. In special crystallographic directions the difference may even vanish completely or fall into the accuracy limits of measurement (e.g. $n_{\gamma,\beta}$-cut of Fe–Cl, Figure 6). Therefore the *m*-phase was overlooked in early investigations of Fe–Cl and Fe–I boracite.[18] More careful measurements led, however, in the case of Fe–Cl, Co–Cl, and Zn–Cl boracite to the observation of a monoclinic phase of point group *m*, intermediate between the *mm*2 and 3*m*-phase[8] (Figures 6, 7 and 15). The *mm*2 → *m* transition is characterized by the splitting up of a *mm*2 single domain state into a package of fine lamellar twins of thickness 1 μm and less, with their composition plane perpendicular to the former *mm*2 polar direction (Figures 18 and 20). This twinning is consistent with point group *m*. For the species $\bar{4}3mFm$ twelve domain orientations are possible, but if one *mm*2 single domain is cooled to the *m*-phase one observes that the crystal—in an attempt at minimizing mechanical and electrostatic energy—chooses only that lamellar twin pair—out of the six possible ones—the monoclinic individuals of which are related by the lost symmetry elements of the original *mm*2 domain. This relationship has successfully been used for interpreting EPR spectra of lamellar packages of Mn^{2+} doped Zn–Cl boracite[19–21].

On further cooling to the 3*m*-phase[17] the monoclinic packages of lamellas transform as a rule into packages of rhombohedral lamellas with the same orientation of the composition planes (Figure 20). For the sake of plausibility, the monoclinic and rhombohedral tilt with respect to the cubic cell, respectively 90°-β and 90°-α', has been exaggerated in Figure 20 (boxes 5, 7), likewise the tilt of the direction of P_s and the extinction directions of the *m*-phase (box 5). In reality, the deviation of the extinction direction in the *m*-phase (box 5) relative to that of the *mm*2 phase (box 3) is hardly perceptible, nor does the conoscopic figure of the lamellar array differ from that of the *mm*2 single domain (Figure 18).

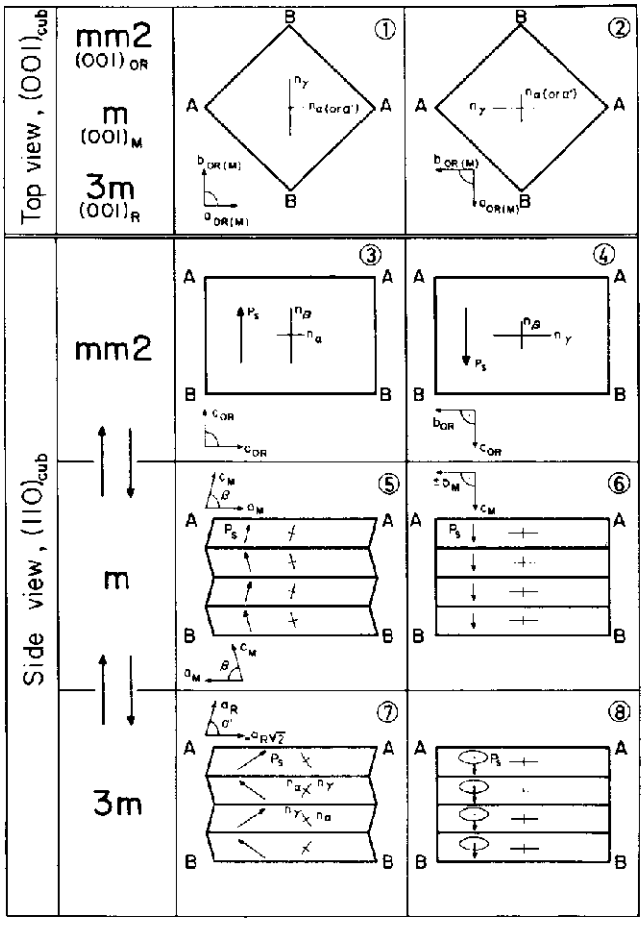

FIGURE 20 Correlation of reversible domain orientations in the transition sequence $mm2 \rightleftarrows m \rightleftarrows 3m$ (deviation of monoclinic and rhombohedral angles β and α', respectively, from 90° is exaggerated).

Owing to high coercive fields of the rhombohedral phases,[17] large $3m$ single domains can be obtained only by electroding and poling very thin (111) cut slabs. These are not adequate for measuring Δn_s in the principal section. Therefore Δn_s of the $3m$ phase of Fe–Cl, Fe–Br and Zn–Cl boracite (Figures 6 and 15) had to be measured on $(110)_{cub}$ cuts on spontaneously formed domains of lamellar form and moderate width. These domains were, however, not necessarily stress/strain free.

4.4 Comments on the Measurement of Spontaneous Birefringence versus Temperature of Individual Compositions

Mg–Cl-boracite The principal birefringences at room temperature have been reported earlier for natural crystals:

$n_{\gamma,\alpha}$: 0.01074			0.010		
$n_{\gamma,\beta}$: 0.00597	white	(22)	0.006	sodium	(23)
$n_{\beta,\alpha}$: 0.00477	light		0.004	light	

Our data at $\lambda = 546$ nm, measured on a natural crystal from Eime–Hannover (Figure 1), are identical with those of Ref. 23. The temperature dependence (Figure 1) of Δn_s is typical for most orthorhombic boracites.

Cr–Cl-boracite Only Δn_s perpendicular to P_s has been measured (Figure 2) by means of a Senarmont compensator and photoelectric detection on a domain stable at zero electric field. Domain stability was, however, a problem for most other Cr–Cl samples (see Section 4.5.4).

Mn-boracites The temperature dependence of Δn_s of Mn–Cl and Mn–Br boracite shows the Mg–Cl type behaviour (Figures 3 and 4), whereas that of $n_{\gamma,\beta}$ ($\perp P_s$) of Mn–I is unusual. The type of the indicatrix of Mn–I is analogous to that of Fe–I (Type B, see Table II). The temperature dependence of $\Delta n_{\gamma,\beta}$ ($\perp P_s$) of Mn–I (Figure 5) does not seem to reflect the temperature dependence of the order parameter, whereas that of $\Delta n_{\gamma,\alpha}$ and $\Delta n_{\beta,\alpha}$ seems to do so. An identical temperature dependence has been obtained by calculation from measured $\Delta n_{\gamma,\alpha}$ and $\Delta n_{\beta,\alpha}$ and from an independent direct measurement on another sample. However, a difference in absolute value subsists (Figure 5) which largely exceeds the accuracy of measurement. It turned out that this effect is caused by an apparent thickness dependence of birefringence, larger values of Δn_s being found for thicker samples. This queer phenomenon is probably not an intrinsic one, but due to a monotonous change in supersaturation of the MnI_2 and I_2 pressure during growth. It needs further study.

Fe-boracites The iron boracites (Figure 6) demonstrate nicely how the magnitude of Δn_s and that of the transition temperatures increase in the sense I-, Br-, Cl-boracite. The thermal hysteresis of all phase transitions—except for the $3m \rightleftarrows m \rightleftarrows mm2$ transitions of Fe–I[24]—was $\leqslant 0.2$ degree owing to good quality of the samples. The indicatrix of orthorhombic Fe–I is of the type B (Table II, Figure 19) with $n_{\beta,\alpha}$ perpendicular to P_s (data with full lines from Ref. 25).

Co-boracites For Co–Cl boracite, only measurements on the $(110)_{cub}$ cut have been made. The difference in Δn_s between the m and $mm2$ phase is extremely small (Figure 7). In a good quality crystal the $m \rightleftarrows mm2$ hysteresis was 0.2 degree or smaller; in less perfect crystals, up to 10 degrees hysteresis was found. It is noteworthy that measurements of

the Mössbauer effect on Co–Cl boracite did not reveal the transition $m \rightleftharpoons mm2$.[26]

For Co–Br boracite, only Δn_s perpendicular to P_s was measurable (Figure 8) because of high coercive fields (Table I). In a poor quality crystal with sector structure, T_c was lower by six degrees in some regions and $\Delta n_s \sim 12$ percent lower than in good crystals.

Co–I boracite is strongly absorbing[27] and has necessitated a small thickness of sample (48 μm) for correctly interpreting the inference order. Domain instabilities required the maintenance of a bias field of 20.6×10^5 Vm^{-1}. The temperature dependence of Δn_s perpendicular to P_s (Figure 9), measured at $\lambda =$ 500 nm, is not unusual but contrasts with that reported[28] for $\lambda = 632.8$ nm, which shows a sign reversal at about −85°C (Figure 9). In order to clarify this point we have measured the dispersion of Δn_s (Figure 10) at −78°C, which is closely below T_c (−75°C). An anomalous dispersion is observed with a maximum of Δn_s peaking around $\lambda \approx 540$ nm. Because of the presence of absorption maxima at about 445 nm and 580 nm[27] measurement below 480 nm and above 560 nm was not possible with an ordinary tungsten lamp. The decrease of Δn_s above 550 nm probably continues with increasing wavelength and may lead to a sign reversal at about 620 nm. This would explain the results reported[28] for $\lambda = 632.8$ nm.

Ni-boracites Measurements of the temperature dependence of Δn_s of Ni–Cl and Ni–Br boracites were performed earlier.[29] In Figures 11 and 12 improved measurements are presented which have been performed on $(110)_{cub}$ cut slabs containing large domains both of $n_{\beta,\alpha}$ and $n_{\gamma,\alpha}$.

The low temperature phase of Ni–I boracite has not been studied. A discussion of the parasitic birefringence of the cubic phase of Ni–I has been published recently.[30]

Cu-boracites The slope of $n_{\gamma,\alpha}$ ($\perp P_s$) with temperature of Cu–Cl boracite (Figure 13) is the steepest one observed among all *mm*2 boracites studied. This reflects a "close to second order" phase transition, also evident from Raman effect[31] and piezoelectric measurements.[32] A strong temperature dependence of spontaneous polarization (high pyroelectric coefficient) was therefore expected, and has been confirmed experimentally[33] (see below). The second order tendency is not found for Cu–Br boracite (Figure 14).

Zn-boracites The behaviour of Zn–Cl boracite is very similar to that of Fe–Cl boracite, except that a larger thermal hysteresis has been found for the former (Figure 15). It is noteworthy that Zn–Cl has the particularity that large crystals in the 3*m* state usually consist of only one stack of lamellas made up of two out of the four possible domain states. This fact facilitated very much the interpretation of EPR data.[20] The behaviour of Zn–Br and Zn–I boracites (Figure 16) conforms to that of the majority of the *mm*2 phases.

Cd-boracites Only tiny samples (<1 *mm*2) with even smaller single domains (narrow-bands) were available for the measurements. Therefore only Δn_s ($\perp P_s$) has been measurable for Cd–Cl, Cd–Br and Cd–I boracite (Figure 17). The observed small and usual temperature dependence does in no way indicate an additional phase transition which was expected to exist on the basis of DTA-measurements[34] in Cd–Cl and Cd–Br, around 298–315°C and 248–270°C respectively.

4.5 *Some Possible Sources of Erroneous Results*

4.5.1 "Forbidden" orthorhombic 180° head-head (tail-tail) domains In some orthorhombic boracites (Mg–Cl, Ni–Cl, Zn–Br) unexpected electrostatically and ferroelastically unallowed 180°C domains with $(001)_{o.r.}$ as composition plane have been observed[35] (Figure 21). They often occur in small depth (e.g. 5 μm) beneath the natural surface of cubic (100) facets. For opposite sense of P_s these domains give rise to an apparently smaller Δn_s perpendicular to P_s. Therefore, testing for symmetric path difference for opposite field polarity is mandatory.

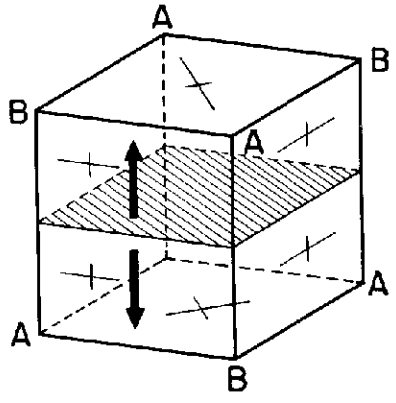

FIGURE 21 "Forbidden" composition plane $(001)_{o.r.}$ of *mm*2 180° head-head (tail-tail) domains.

4.5.2 Superposition of growth sectors Often different growth sectors having different Curie temperatures are superposed in a sample. This situation may lead to steps in the Δn_s (T) curve (e.g. Co–Br). The most spectacular difference in Curie temperature among different growth sectors has been observed for Cu–Br boracite:

clear (100) sector: T_c = −33.3°C (cooling), −30.0°C (up heat),

dark (111) sector: T_c = −43.1°C (cooling), −38.2°C (up heat).

The very low T_c (−53°C) reported elsewhere[36] may be due to a (111) sector grown under somewhat different conditions.

4.5.3 Superposition of allowed 180°C domains Poled $(110)_{cub}$-cut platelets may appear homogeneous on the (110) facet. In reality spike like domains with antiparallel polarisation may be visible

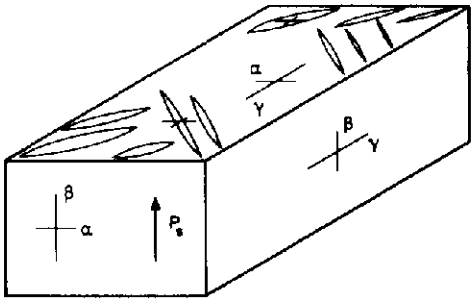

FIGURE 22 Normal *mm*2 180° domain spikes disturbing Δn_s measurements on $(110)_{cub}$ cuts.

on tilting the sample by 90° and observing along P_s. Nucleation of spikes from and propagation at 45° to (110) facets is frequent (Figure 22) for the field free state.

4.5.4 Anomalous temperature—electric field—phase diagram In some crystals of Cr–Cl boracite an anomalous switching behaviour in the electric field was observed. In Figure 23, it is shown that a $(100)_{cub}$ cut platelet with P_s perpendicular to its large facet undergoes between −90 and −120°C a spontaneous switching of P_s into the plane of the platelet if cooled down in zero electric field. The phenomenon is reversible on upheat. At a fixed temperature, e.g. −40°C, the same sequence of states can be run through by increasing and decreasing the electric field strength. The location of the frontiers delimiting the regions A, B, C differs from crystal to crystal. For the majority of Cr–Cl crystals state A is stable at any field strength

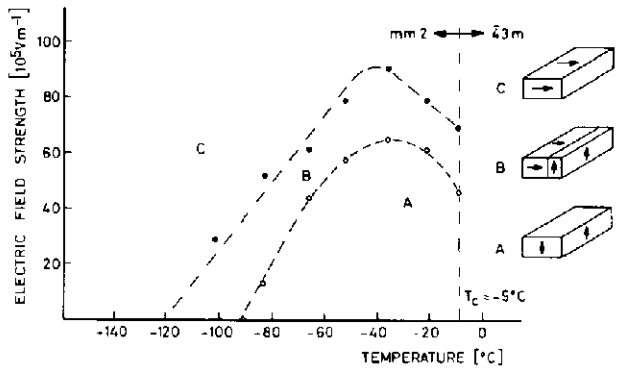

FIGURE 23 Phase diagram "temperature/electric field strength" of anomalous *mm*2 $Cr_3B_7O_{13}Cl$.

(including zero) and at any temperature (normal behaviour).

In some boracites the reverse situation on Figure 23 has been observed, i.e. region C coming dow into the zero and small field strength region and region A shifting up to high field strength (e.g. Ni–Br, Cu–Cl). This would be the sequence expected in an electric field, whereas that of Cr–Cl is unusual. Growth-induced anisotropies are probably causing the great variety of anomalous behaviour.

4.5.5 Apparent thickness dependence of Δn_s As shown for Mn–I boracite, Δn_s depends on thickness. This effect is probably caused by variations of the synthesis gas composition. It merits further study. Small Δn_s compositions (I-boracites) may be particularly affected.

4.5.6 Temperature gradient If too thick crystal platelets are used (≥0.4 mm) the orthorhombic-cubic transition may appear of second order because of slow propagation of the $\bar{4}3m/mm2$ phase boundary in the direction of a thermal gradient along the microscope axis.

The examples of error sources (Sections 4.5.1 t 4.5.6) show that utmost care is required for measuring Δn_s and other properties of single domains.

5 APPLICATIONS OF SPONTANEOUS BIREFRINGENCE

5.1 Information on the Temperature Dependence of the Order Parameters

In order to explain the origin and temperature dependence of the measured Δn_s data and to check current phenomenological theories, a knowledge of the electro-optic and piezo-electric coefficients,

spontaneous polarization, deformation, etc. would be necessary. Owing to absence of such data, only some rudimentary statements can be made:

The phase relationship cubic-trigonal ($T_d^5 - C_{3v}^6$) of boracites is proper.[17,37] Thus spontaneous polarization P_s is the order-parameter and Δn_s ($= n_\gamma - n_\alpha$) can be expressed (see e.g. Refs. 38 and 39) in terms of P_s, the linear and quadratic electro-optic coefficients, f_{41}^p and g_{44}^p, respectively) of the cubic phase and the refractive index n_o of the cubic phase:

$$n_{s(\gamma,\alpha)} = -\frac{\sqrt{3}}{2} n_0^3 f_{41}^p P_s - \tfrac{1}{2} n_0^3 g_{44}^p P_s^2 \qquad (1)$$

The coefficients f_{41}^p and g_{44}^p are understood to contain the direct and elasto-optic contributions. The quadratic term being probably smaller than the linear one, $\Delta n_s(T)$ of the trigonal phase is supposed to reflect essentially $P_s(T)$.

If the phase relationship $T_d^5 - C_{2v}^5$ in boracites would be of the proper type, the three principal Δn_s values of the orthorhombic phase would take the following form if spontaneous elasto-optic contributions owing to P_s-independent components of spontaneous strain are disregarded for reasons of simplicity:

$$\Delta n_{S(1,2)}(\perp P_s) \cong -n_0^3 f_{41}^p P_{S(3)} \qquad (2)$$

$$\Delta n_{S(1,3)} \cong \tfrac{1}{2} n_0^3 f_{41}^p P_{s(3)} + \tfrac{1}{2} n_0^3 P_{s(3)}^2 (g_{11} - g_{12}) \qquad (3)$$

$$\Delta n_{S(2,3)} \cong -\tfrac{1}{2} n_0^3 f_{41}^p P_{s(3)} + \tfrac{1}{2} n_0^3 P_{s(3)}^2 (g_{11} - g_{12}) \qquad (4)$$

However, the $T_d^5 - C_{2v}^5$ transition of boracites is improper. Thus P_s is no longer the primary order parameter. Therefore, Smutny and Koňák[28] take account of contributions from the transition parameter q_1, q_2 to the polarization constant B_6:

$$\Delta B_6 = \omega_1 q_1 q_2 + \omega_2 P_{s(3)} (q_1^2 + q_2^2) + f_{41}^p P_{s(3)} \qquad (5)$$

where the coefficients are temperature independent. Equation (2) thus takes the form

$$\Delta n_{s(1,2)}(\perp P_s) = -n_0^3 \Delta B_6 = -n_0^3 (f_{41}^p - D') P_{s(3)} \qquad (6)$$

where D' describes the improper contribution:

$$D' = \frac{\omega_1 + 2\omega_2 P_{s(3)}}{\chi_p(\mu + 2\gamma P_{s(3)})}. \qquad (7)$$

Here ω_1, ω_2, μ and γ are coefficients of the thermodynamic potential[28] and χ_p the susceptibility. Analogous correction terms will be required for the linear and quadratic terms of Eqs. (3) and (4). In case of negligible improper contributions, Eqs. (2), (3) and (4) are probably a good approximation.

Experiment shows that for orthorhombic Co–Cl, Cu–Cl, Zn–Cl and Zn–Br boracites (Figures 7, 13, 15 and 16) $\Delta n_{s(2,3)}$ and $\Delta n_{s(1,3)}$ (i.e. $n_\gamma - n_\beta$ and $n_\beta - n_\gamma$) are nearly equal in magnitude, opposite in sign and nearly half the value of $\Delta n_{s(1,2)}$ (i.e. $n_\gamma - n_\alpha$) as required by the linear terms alone of Eqs. (2), (3) and (4), and as manifested by indicatrix type A (Figure 19a). The relative importance of the terms linear in $P_{s(3)}$ of Eqs. (3 and 4) decreases (see e.g. Figure 6) in the sense Cl → Br → I-boracite, leading finally to a situation where $\Delta n_{s(1,2)}$ ($\perp P_s$) lies in between $\Delta n_{s(1,2)}$ and $\Delta n_{s(1,3)}$ as manifested by indicatrix type B (Figure 19a). Fe–I and Mn–I boracites are examples of the latter type (Figures 5 and 6). For the time being it is not possible to decide whether this tendency is due to an increasing relative importance of improper contributions, to the spontaneous quadratic electro-optic terms, or to both of them.

5.2 *Simultaneous Visual Control of the Domain State During Crystallophysical Measurements*

Verification of current theories of phase transitions (e.g. for improper ferroelectrics) requires most reliable data on the tensorial properties of many crystallophysical phenomena as a function of temperature, such as susceptibilities, elastic and piezoelectric coefficients, spontaneous polarization, etc. Going through the literature and checking the reliability of published data, the present-day situation for boracites appears as alarming. The main reason is the neglect by many workers of simultaneous visual control of the domain state, which has proved indispensable throughout the *entire* temperature range of measurement. For that purpose an exact knowledge of the indicatrix properties is mandatory.

As an example, let us discuss reported measurements of spontaneous polarization of boracites: all available data have been collected in Table III. It can be seen that in those cases where the magnitude and orientation of Δn_s has been used to check the single domain state *during* the measurements (Co–I,[28] Fe–I,[40] Cu–Cl[33] and Cu–Br[33]), the spontaneous polarization is of the order of 1 to 4 μ Cb cm^{-2}. This is in good agreement with the predicted upper limit

TABLE III

Data of spontaneous polarisation in boracites (comparison of results with and without visual control of domain state)

Boracite	P_s [10^{-2} C m^{-2}]	Temperature [°C]	Method	Optical control during measurement	Thickness [μm]	Comments	References
Mg–Cl	≥ 0,002	25	Sawyer–Tower (200 – 265°C)	insufficient	1400		42
	0,075 0,035 (minimum) 0,09	– 173 127 267 (T_c)	$\partial P_s/\partial T$ (dynamic) + P_s at T_c (static)	insufficient	800	P_s at T_c on detwinned(?) crystal; $\partial P_s/\partial T$ on partially twinned crystal	43
	∿ 0,085 ∿ 0,075	∿ 207 265 (T_c)	$\partial P_s/\partial T$	not reported	500		44
	∿ 0,078 ± 15% ∿ 0,070 ± 15%	245 265 (T_c)	$\partial P_s/\partial T$ static, P_s by integration	not reported		"domain structure: coefficient of unipolarity close to unity"	45
	0,07 0,09	265 T_c 230	pyroelectric	not reported	300		46
Cr–Cl	0,0003	–8 to –10(T_c)	$\partial P_s/\partial T$ static, P_s by integration at T_c	not reported	?	$\partial P_s/\partial T = 0$	47
	0,0003			not reported	90		44
Fe–Br	0,35 (3m) 0,22 (m2)	47 – 127 127 – 227	$\partial P_s/\partial T$ static, P_s by integration	not reported	180		44
	0,22 (3m) 0,15 (m2)	100 – 130 130 – 227	idem	none			48
Fe–I	3,9 ± 0,1 3,7 ± 0,1	25 72 (T_c)	1) Sawyer–Tower 2) Camlibel-pulse method 3) pyroelectric current (20–72°C) 4) P_s at T_c by charge integration of jump	yes	100		40
Co–Cl	0,06 (3m) 0,02 (m2)	150 270 – 330	$\partial P_s/\partial T$ static	none	?		48
Co–I	≥ 1,5	– 73 (T_c)	ultra-slow hysteresis cycle (4 x 10^{-4} Hz)	none	150		67
	1,7	≤ –73 (T_c) T independent	idem	yes	100 – 200		28
	0,4	– 73 (T_c)	$\partial P_s/\partial T$ static	some		measurements on multidomain samples	36
Ni–I	0,08 (// [001])	4°K	Sawyer–Tower (50 Hz) on (110)-cut	not reported	?		49
Cu–Cl	1,85 (meas.) 1,74 (meas.) 1,00 (extr.)	20 43 96 (T_c)	Camlibel pulse method	yes	79		33
Cu–Br	3,2 2,6 – 3,0	–110 – 35	Camlibel pulse method	yes			33
	0,47 0,51	4°K ∿ –123	$\partial P_s/\partial T$ static	some		measurements on multidomain samples	36

of P_s of about 5 μ Cb cm^{-2} for "3-dimensional ferroelectrics"[41] to which the boracites belong. Many of the published P_s data—collected without or with insufficient optical control—fall, however, short *by one to four orders of magnitude* (Mg–Cl,[42–46] Cr–Cl,[44,47] Fe–Br,[44,48] Co–Cl,[48] Co–I,[36] Ni–I,[49] Cu–Br.[36] This does not seem to be accidental.

The discrepancy between the measurements of P_s with and without control of Δn_s can be well seen for Co–I and Cu–Br boracite (Table III) and for measurements of P_s of Cu–Cl-boracite with Camlibel's pulse method.[33,50] In the latter case, P_s follows the curve $P_s = P_s$ (20°C) $\Delta n(T)/\Delta n$(20°C) from 20 to 40°C; thereabove, P_s falls off apparently, which is due to visually observed backswitching and concomitant ill-defined initial and final domain patterns.

The polarizability of all 3*d*-transition metal ions is very similar, the structure of the cubic phases,[51] and that of the orthorhombic phases[52] is similar, and so is Δn_s among the chlorine, Δn_s among the bromine and Δn_s among the iodine boracites (Figures 1–17). It is therefore likely that many of the reported P_s-data (Table III) will turn out to be much higher when careful optical control is applied during P_s measurements.

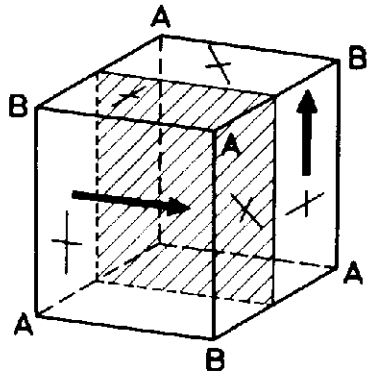

FIGURE 24 Frequently occurring domain configuration in Fe–I boracite leading to optical cross-talk if P_s within plane of platelet.

5.3 *Information on the Statics and Dynamics of Domains*

Because boracites are fully ferroelectrics/fully ferroelastics, the optical indicatrix is oriented differently for all possible domain states. All domain states can therefore be distinguished by magnitude or orientation of Δn_s using orthoscopic or conoscopic techniques:

5.3.1 Static domain patterns of some boracites have been studied, based on this principle for the *mm*2 phase[29,35]) 3*m*-phase[17,53] and *m*-phase (see Sections 4.2 and 4.3, Figure 18 and 20 and the review[54]).

5.3.2 Effects of ferroelasticity The contrast due to Δn_s between orthorhombic 180° and 90° domains on $(100)_{cub}$-cuts has been used to study the influence of the magnitude of the ferroelastic shear angle α† on the switching behaviour of Fe–I boracite.[55] One important conclusion: domains, being embedded in an antiparallelly poled matrix, switch back elastically for shear angles above ~2 minutes. Sometimes the crystal avoids the elastic back-switching—without breaking—by accommodating the ferroelastic stress by the formation of spikes having P_s in the plane of the platelet (Figure 24). This phenomenon leads, however, to optical cross talk.[55]

5.3.3 Studies of the domain wall velocity The good contrast—due to 90°—rotation of the indicatrix—between 180° domains for (001) cut orthorhombic Fe–I has been used to study elegantly and rapidly the domain wall velocity vs. field and temperature by means of photoelectric detection.[55] It has been shown that the velocity of 180° domain walls is an exponential function of the reciprocal electric field strength,[55] a law which has also been found for the optically indistinguishable 180° domain walls of $BaTiO_3$[56–59] by means of a laborious etching technique. The exponential law simply means that there is no threshold field for switching.

† Definition: $\alpha \equiv |90° - 2\,tg^{-1}a/b|$.

TABLE IV

Phase transition temperature [°K] of some boracites as determined by measuring Δn_s

	$\bar{4}3m$ ++ $mm2$	$mm2$ ++ m	m ++ $3m$	$mm2$ ++ $3m$		$\bar{4}3m$ ++ $mm2$	$mm2$ ++ m	m ++ $3m$
Mg–Cl	536† 538†				Ni–Cl	608† 610†		
Cr–Cl	264				Ni–Br	398† 399†		
Mn–Cl	680							
Mn–Br	543				Cu–Cl	369		
Mn–I	407				Cu–Br	243		
Fe–Cl	609	543	528		Zn–Cl	723	564† 567†	472† 480†
Fe–Br	495			405	Zn–Br	585		
Fe–I*	349	203† 218†	191† 205†		Zn–I	379		
Co–Cl	623	538	468		Cd–Cl	795† 797†		
Co–Br	466				Cd–Br	733† 735†		
Co–I	190† 198†				Cd–I	633† 635†		

5.4 *Potential Components for Optical Page-Composers, Optical Storage and Passive Display*

With the advent of the idea put forward by Rajchmann (see e.g. Ref. 60) of the "optical computer" a feverish search for components thereof, such as page-composers and holographic storage materials, began in laboratories all over the world. Ferroelectrics permitting optical contrast upon switching were considered as one of the potential solutions, e.g. as a photoconductor/ferroelectrics sandwich for bidimensional holographic storage, or as an electrically matrix-addressed page-composer. In this context especially $Bi_4Ti_3O_{12}$, $Gd_2(MoO_4)_3$ (GMO), $Pb_5Ge_3O_{11}$ and PLZT-type materials have been studied. For a detailed discussion of advantages and disadvantages of these materials, see Ref.[61]. As regards boracites, the following advantages sprang to the eye: (i) high Δn_s, permitting thin $\lambda/4$ wave plates (e.g. 7 μm for Ni–Cl boracite),

hence allowing in principle small addressing voltages, (ii) small ferroelectric shear angle, avoiding cracking, etc., and (iii) advantageous symmetry permitting a 90° rotation of the elliptic indicatrix cross section, thus allowing a 100% light transmission in the "on" state, if reflection losses are disconsidered. This is why a study of the optical memory properties of Fe–I boracite single crystals and a feasibility study of synthetizing layers of Ni–Cl boracite have been undertaken at Battelle–Geneva.

5.4.1 Single crystal studies on Fe–I boracite Since Δn_s ($\perp P_s$) of Fe–I boracite is about 0.004 at room temperature, $\lambda/4$ wave plates can be made with 34 and 17 μm thickness for transmission and reflection, respectively, and addressing voltages 10× smaller than for GMO are possible because Δn_s ($\perp P_s$) = 0.0004 for the latter one. It has been shown that fatigue free switching is possible for isolated memory elements, for at least 10^8 cycles, but that mechanical and optical crosstalk effects do not allow a cross-bar access owing to the finite ferroelectric shear-angle of about 2 min.[55] Arrays of stripe-like elements can, however, be operated satisfactorily, as is the case for GMO.[62,63]

5.4.2 Studies of epitaxial layers of Ni–Cl boracite on Cr–Cl boracite For industrial application, the preferable form of an optical component of boracite would be a "thick" layer. Therefore the feasibility of chemical deposition of boracite layers has been successfully studied.[64] For the system orthorhombic Ni–Cl boracite on cubic Cr–Cl boracite as substrate, it has been shown that layers between 2 and 100 μm thickness can be produced by CVD using a closed (ampulla) or an open (continuous flow) system. Good contrast 180° domains with a size down to $\leqslant$1 μm have been achieved.

5.4.3 Suggestions for future developments It has been demonstrated[55,61,64] that the key requirement for using the switching of Δn_s of boracites—as well as of any other ferroelastic ferroelectric—is the development of a composition having a zero or a tiny shear angle ($\leqslant$1 min of arc) in order to prevent cracking, elastic back-switching, optical and mechanical cross-talk, fatigue, etc., and in order to allow poly-nucleation which leads to short switching times of a memory element of a given size.[54] We can see three ways of approach in order to realize such desirable "shear free" or "shear-poor" compositions of boracites:

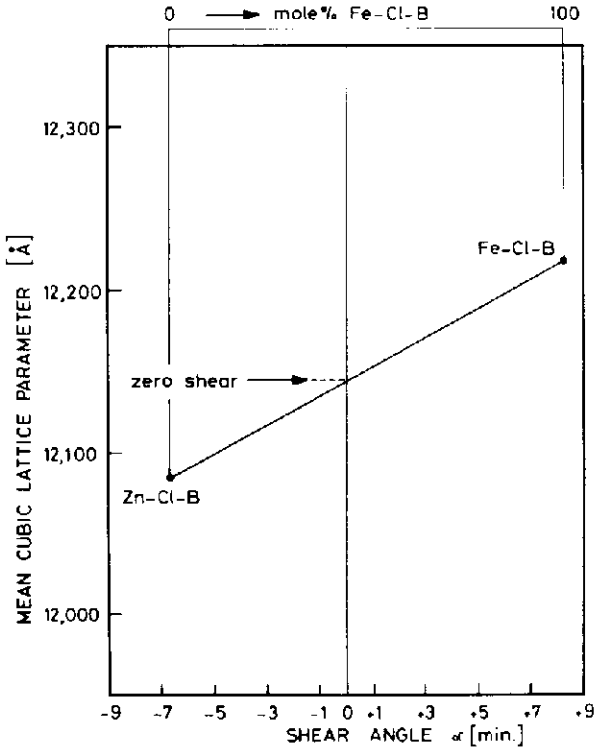

FIGURE 25 Location of zero shear angle composition in the rhombohedral pseudo-binary system Zn–Cl/Fe–Cl boracite (schematic).

i) The *trigonal phase* of Zn–Cl boracite on the one hand, and that of Fe–Cl and Fe–Br boracite on the other hand, have opposite shear relative to the boron-oxygen skeleton.[17] Therefore, at a given Zn–Fe ratio and at a given temperature, a zero shear composition must exist (Figure 25) in the pseudo-binary phase diagram of Fe–Cl/Zn–Cl and Fe–Br/Zn–Cl boracite. Figure 20 (boxes ①–② and ⑦–⑧) depicts the geometry allowing contrast.

ii) In the *mm2 phase* of Fe–I boracite the shear angle approaches zero when the temperature approaches that of the transition $mm2 \rightleftarrows m \rightleftarrows 3m$.[24,65] Operation in the *mm*2 phase close to the transition to the *m*-phase is characterized by absence of back-switching and by poly-nucleation.[55] By synthesizing mixed crystals (e.g. Fe–I/Fe–Br) it may be possible to shift the small shear region to room temperature.

iii) Possibly there exist different orthorhombic boracite compositions having shear of opposite sign relative to the boron-oxygen skeleton as do the trigonal phases. (Zn/Fe boracite pairs are potential candidates.) If the switching of any ferroelastic/ferroelectric boracite is ever to be used technologically, the development of the production of

layers or of large single crystals is mandatory. For reasons of symmetry the substrate for layers has, however, to have a binary axis perpendicular to its surface in order to achieve contrast.

5.5 *Studies of Surface Layers and Defects*

Spontaneous birefringence has been successfully used to visualize surface layers of about 5 μm thickness of Ni–Cl boracite, which behave dynamically differently from the bulk crystal and are probably due to a change of supersaturation during the cooling phase of the growth.[35] It would be rewarding to study the surface layers in boracites and other ferroelectrics permitting direct visualization via Δn_s owing to favorable symmetry. This might shed more light on the still very obscure problem of surface layers of ferroelectrics in general (see e.g. Ref. 66).

6 CONCLUSIONS

It has been shown that measurement of spontaneous birefringence *vs.* temperature is a simple but sensitive and powerful means of studying phase transitions, twinning and defects in boracites, even more sensitive in many cases than x-ray analysis and Mössbauer spectroscopy.

The results presented for twenty-one boracite compositions are expected to be useful for obtaining information on the order parameters' temperature dependence, although they will still have to be complemented by measurements of electro-optic and elasto-optic coefficients, spontaneous polarization, etc., before definite conclusions on the various contributions to Δn_s can be drawn.

The symmetry properties of the boracite species $\bar{4}3mFmm2$, $\bar{4}3mFm$ and $\bar{4}3mF3m$ are unique in the sense that they allow optical contrast in a longitudinal mode upon switching of P_s or of a component thereof along $[001]_{cub}$. Chemical and physical feasibility studies show that these properties may be exploited technologically, but more development work would be required with respect to the synthesis of shear free compositions in the form of layers or of large single crystals. The most important present-day application of spontaneous birefringence of boracites—as well as that of other ferroelastic ferroelectrics—lies in the field of research: control of the domain state at any temperature of measurement of crystallophysical properties cannot sufficiently be recommended to all workers in the field. Why deny the use of a pattern recognition machine with a computer on line? There exists a priceless, simple, but marvellous system which is ready for most of you: a polarizing microscope plus your eyes, plus your brains!

ACKNOWLEDGEMENTS

Thanks are due to Professor Saalfeld/Hamburg University for providing natural Mg–Cl boracite crystals, at Battelle-Geneva to G. Kliegl and L. A. Pétermann for some help in birefringence measurements, and to H. Guédu for help in electroding samples and growing crystals. J.-P. Rivera, University of Geneva, kindly provided unpublished data on Buerger precession photographs.

The work presented in this paper extends over a couple of years and has profited from various sources of support: Thomson CSF/France, Montecatini/Italy, Rank Precision Industries/England, Délégation à l'Informatique/Paris, DRME/Paris, Battelle Institute/Columbus, Battelle-Geneva Research Centre. The authors extend their gratitude to all of them.

REFERENCES

1. R. J. Nelmes, *J. Phys. C: Solid State Phys.* **7**, 3840 (1974).
2. Gmelin, *Handbuch der anorganischen Chemie, New Supplement Series to 8th Ed.*, Vol. 28, pp. 198–205 (1975) Springer.
3. Landolt-Börnstein, *Numerical Data and Functional Relationships in Science and Technology, New Series, Group III*, Vol. 3 (Springer, 1969) p. 115.
4. T. A. Bither and H. S. Young, *J. Solid State Chem.* **10**, 302 (1974).
5. W. Jeitschko, P. E. Bierstedt and T. A. Bither, *Third European Crystallographic Meeting, Zürich*, 6–10 Sept. 1976, Abstract Booket, pp. 369–71.
6. J.-M. Reau, A. Levasseur, G. Magniez, B. Cales, C. Fouassier and P. Hagenmuller, *Mat. Res. Bull.* **11**, 1087 (1976).
7. K. Aizu, *Phys. Rev.* **B2**, 754 (1970).
8. H. Schmid, G. Kliegl and J. Kobayashi, *Helv. Phys. Acta* **42**, 599 (1969).
9. H. Schmid, *Int. J. Magnetism* **4**, 337 (1973).
10. C. Hintze, *Handbuch der Mineralogie, I, 4 Abt.* (Berlin–Leipzig, 1933) pp. 104–128.
11. G. H. O. Volger, *Versuch einer Monographie des Borazites* (Carl Rümpler, Hannover, 1855).
12. J. W. Mellor, *A Comprehensive Treatise on Inorganic and Theoretical Chemistry*, Vol. V (Longmans, Green & Co., New York, 1924).
13. H. Schmid, *J. Phys. Chem. Solids* **26**, 973 (1965).
14. J.-P. Rivera, University of Geneva, private communication (1974).
15. J. Kobayashi, H. Schmid and E. Ascher, *Phys. Stat. Sol.* **26**, 277 (1968).
16. J. Gahm, *Quantitative polarisationsoptische Messungen mit Kompensatoren, Zeiss-Mitteilungen* **3**, 153 (1964).
17. H. Schmid, *Phys. Stat. Sol.* **37**, 209 (1970).
18. H. Schmid and J. M. Trooster, *Solid State Comm.* **5**, 31 (1967).

19. J. P. Rivera, Thèse de Doctorat, University of Geneva (1976).
20. J.-P. Rivera, H. Bill and R. Lacroix, *Ferroelectrics* **13**, 363 (1976).
21. J.-P. Rivera, University of Geneva, unpublished.
22. E. Mallard, *Bull. Soc. Fr. Min.* **6**, 129 (1883).
23. E. M. Guppy, *Min. Mag. and J. of the Mineral Soc.* **27**, 51 (1944).
24. J. Kobayashi, Y. Sato and H. Schmid, *Phys. Stat. Sol. (a)* **10**, 259 (1972).
25. J. Kobayashi, I. Mizutani, H. Hara, N. Yamada, O. Nakada, A. Kumada and H. Schmid, *J. Phys. Soc. Jap. (Suppl.)* **28**, 67 (1970).
26. I. S. Zheludev, T. M. Perekalina, V. G. Pyl'nev, E. M. Smirnovskaya, V. F. Belov, A. M. Kostsov and Yu. N. Yarmukhamedov, *Izv. Akad. Nauk SSSR. Ser. Fiz.* **39**, 724 (1975).
27. R. V. Pisarev, V. V. Druzhinin, S. D. Prochorova, N. N. Nesterova and G. T. Andreeva, *Phys. Stat. Sol.* **35**, 145.
28. F. Smutný and C. Koňák, *Phys. Stat. Sol (2)* **31**, 151 (1975).
29. H. Schmid, *Rost Kristallov* 7, 32 (1967).
30. R. J. Nelmes and F. R. Thornley, *Ferroelectrics* **13**, 355 (1976).
31. D. L. Lockwood and R. W. G. Syme, *4th International Meeting on Ferroelectricity*, Leningrad, Sept. 1977.
32. P. Genequand, H. Schmid, G. Pouilly and H. Tippmann, *J. Physique*, in press.
33. P. Genequand, H. Schmid and G. Pouilly, Battele Geneva Research Centre, Internal Report (1975), unpublished.
34. T. Takahashi and O. Yamada, *J. Crystal Growth* **33**, 361 (1976).
35. A. Zimmermann, W. Bollmann and H. Schmid, *Phys. Stat. Sol. (a)* **3**, 707 (1970).
36. S. N. Drozhdin, B. G. Bochkov, N. D. Gavrilova, T. V. Popova, V. A. Koptsik and V. K. Novik, *Kristallografiya* **20**, 854 (1975) [*Sov. Phys. Crystallogr.* **20**, 526 (1976)].
37. J.-P. Rivera, H. Bill and R. Lacaroix, *4th International Meeting on Ferroelectricity*, Leningrad, Sept. 1977.
38. S. Namba, *J. Opt. Soc. Am.* **51**, 76 (1961).
39. S. H. Wemple and M. Didomenico, Jr. *Applied Solid State Science*, Vol. 3 (Academic Press, 1972), p. 263.
40. H. Schmid, P. Chan, L. A. Pétermann, F. Teufel and M. Mändly. *Ferroelectrics* **13**, 351 (1976).
41. S. C. Abrahams and E. T. Keve, *Ferroelectrics* **2**, 129 (1971).
42. Y. Le Corre, *J. Phys. Radium* **18**, 629 (1957).
43. L. P. Toore, S. C. Abrahams and R. L. Barns, *Ferroelectrics* **4**, 291 (1972).
44. V. G. Bochkov, V. I. Bugakov, K. A. Verkhovskay, T. M. Polkhovskaya and V. M. Fridkin, *Fiz. Tverd. Tela* **16**, 1863 (1974) [*Sov. Phys. Solid State* **16**, 1217 (1975)].
45. B. G. Bochkov, N. D. Gavrilova, V. A. Koptsik and V. K. Novik, *Neorganicheskie Materialy* **11**, 1522 (1975) [*Inorgan. Materials* **11**, 1301 (1976)].
46. B. G. Bochkov, N. D. Gavrilova, V. K. Novik and V. A. Koptsik [*Sov. Phys. Cryst.* **20**, 404 (1975)].
47. B. G. Bochkov and S. N. Drozhdin, *Kristallographiya* **19**, 1301 (1974) [*Sov. Phys. Cryst.* **19**, 811 (1975)].
48. B. G. Bochkov, N. D. Gavrilova, V. A. Koptsik, V. K. Novik and V. I. Bugakov, *Neorganicheskie Materialy* **12**, 634 (1976).
49. T. Miyashita and T. Murakami, *J. Phys. Soc. Jap.* **29**, 1092 (1970).
50. I. Camlibel, *J. Appl. Phys.* **40**, 1690 (1969).
51. R. J. Nelmes and F. R. Thornley, *J. Phys. C. Solid State Phys.* **7**, 3855 (1974).
52. F. R. Thornley, R. J. Nelmes and N. S. J. Kennedy. *Ferroelectrics* **13**, 357 (1976).
53. B. G. Bochkov, S. M. Bugrov, N. D. Gavrilova, V. A. Koptsik and V. K. Novik, *Kristallografiya* **20**, 851 (1975) [*Sov. Phys. Cryst.* **20**, 524 (1976)].
54. J. Fousek and V. Janovec, *J. Appl. Physics* **40**, 135 (1969).
55. L. A. Pétermann and H. Schmid, *Revue de Physique Appliquée* **11**, 441 (1976).
56. R. C. Miller and A. Savage, *Phys. Rev. Lett.* **2**, (1959).
57. R. C. Miller and A. Savage, *Phys. Rev.* **115**, 1176 (1959).
58. R. C. Miller and A. Savage, *J. Appl. Phys.* **31**, 662 (1960).
59. R. C. Miller and G. W. Weinreich, *Phys. Rev.* **117**, 1460 (1960).
60. J. A. Rajchmann, *J. Appl. Phys.* **31**, 1376 (1970).
61. H. Schmid and H. Schwarzmüller, *Ferroelectrics* **10**, 283 (1976).
62. A. Kumada, *Ferroelectrics* **3**, 115 (1972).
63. A. Kumada, *IEEE Trans. Electron Devices* **ED-20**, 866 (1973).
64. H. Schmid, H. Tippmann and J. Figar, unpublished.
65. J. Kobayashi, I. Mizutani, H. Schmid and H. Schachner, *Phys. Rev.* **B1**, 3801 (1970).
66. E. Fatuzzo and W. L. Merz, *Ferroelectricity* (North-Holland Publ. Comp., Amsterdam, 1967).
67. F. Smutny and J. Fousek, *Phys. Stat. Sol.* **40**, K13 (1970).